GNSS-Based Passive Bistatic Radar for Micro-Doppler Analysis of Helicopter Rotor Blades

CARMINE CLEMENTE, Member, IEEE
JOHN J. SORAGHAN, Senior Member, IEEE
University of Strathclyde
UK

The alternative use of the Global Navigation Satellite System (GNSS) has recently initiated a number of studies that aim to exploit this system as an illuminator of opportunity for a passive radar system. A passive bistatic radar (PBR) configuration using a GNSS as illuminator in near forward scattering zone for micro-Doppler analysis is proposed. It is known that the received signal power is the main issue for this kind of passive radar. It is demonstrated that the enhancement achievable in received signal power strength when operating in a forward scattering mode can cope with this issue. The analysis focuses on the case of helicopters rotor blades where the Doppler shift is very high and a relatively large wavelength is useful in reducing the maximum Doppler shift. The power budget analysis for this kind of configuration and target is presented. This work demonstrates the possibility of detecting these kinds of targets and to measure their micro-Doppler signatures. The theoretical analysis is supported with simulations that demonstrate the effectiveness of the proposed configuration for micro-Doppler signature analysis for helicopter rotor blades.

Manuscript received January 10, 2012; revised August 2, 2012, April 30, 2013; released for publication June 7, 2013.

IEEE Log No. T-AES/50/1/944803.

DOI. No. 10.1109/TAES.2013.120018.

Refereeing of this contribution was handled by C. Baker.

This work was supported by the Engineering and Physical Research Council (Grant EP/H012877/1), the MOD University Defence Research Centre in Signal Processing and Selex-Galileo Edinburgh.

Authors' address: Dept. of Electronic and Electrical Engineering, University of Strathclyde, 204 George Street, Glasgow, Gl 1XW, United Kingdom. E-mail: (carmine.clemente@strath.ac.uk)

I. INTRODUCTION

The study of possible secondary applications of the Global Navigation Satellite System (GNSS) has lead to several remote sensing applications [1, 2]. Interest in exploiting GNSS for remote sensing is growing recently due to the advantage offered by its high coverage in time of the entire Earth.

Exploitation of the GNSS for target detection has been reported in [3–5] and imaging in [6], however the main limitation is identified in the very low power at the receiver. A possible solution to this issue is the use of high gain receiver antennas and a relatively big integration time [3] facilitating a good maximum operative range to be obtained.

In forward scattering the diffracted signal power may be many times higher than the backscattered signal [7]. This effect can be translated as an enhancement of the radar cross section (RCS), known as forward scattering enhancement. This effect can be exploited to cope with the very low power of the received signal in a GNSS-based passive bistatic radar (PBR) [2, 8] opening it to the use of a new family of PBR working in near forward scattering zone [9, 10].

Target micro-motions like vibrations due to the engine or a rotating antenna introduces micro-Doppler components in the received radar signal [11, 12]. These may be extracted from both monostatic and bistatic radar providing some interesting advantages in the bistatic case [12–14]. Bilik et al. in [15], [16] demonstrated the possibility to use micro-Doppler signatures for target recognition using statistical-based tools for the feature extraction and classification. An alternative technique using time warping was proposed in [17] to classify targets for automatic target recognition (ATR) using micro-Doppler, achieving a good level of confidence on real datasets. Of particular interest in the paper is the analysis of the effect from the rotating rotor blades of a helicopter since the effect on the radar returns depends on the characteristics of the rotor, like the blade rotating velocity, blade length, and the number of blades [12, 18]. In [19] it was demonstrated that it is possible to estimate the parameters of helicopters rotor blades for noncooperative target recognition with an algorithm based on the Radon transform. This algorithm was tested on real data and shown to be accurate and able to recognize different helicopters. This technique is not system dependent and could be applied to the system that is presented in this article.

In this paper we investigate the possibility of exploiting the GNSS signal in a PBR system when a target is in the near forward scattering zone for micro-Doppler analysis. The feasibility study will first deal with the constrains of the GNSS system in terms of available pulse rate frequency (PRF) that can form a limitation for the maximum Doppler shift to be analysed correctly. It is shown that as a result of using the 1.5 GHz GNSS signal in a bistatic configuration, the maximum micro-Doppler

shift from the rotating blades is reduced, thus allowing the time-frequency analysis with the standard GNSS PRF of 1 kHz without aliasing. In addition the ambiguity function (AF) for the used waveform is discussed. The second aspect to analyse is the power budget of the received echoes to the receiver from this kind of target. The power budget is presented and it is shown that exploiting the forward-scattering enhancement will allow us to obtain sufficient forward-scattered power to detect the echoes from the rotor blades within certain ranges reducing also the effect of the direct signal interference.

The remainder of paper is organized as follows. Section II introduces the PBR GNSS geometry and the signal model. Section III analyses the micro-Doppler effect from helicopters rotor blades in radar and Section IV analyses the system requirements to correctly perform the micro-Doppler analysis of rotor blades. Section V introduces the forward scattering enhancement concept with a particular attention to the case of the rotor blades, while in Section VI the power budget analysis for the proposed system and for the micro-Doppler analysis purpose is performed. Section VII introduces the processing method to obtain the micro-Doppler signature of the rotating blades. Results of simulations are included for different helicopters. Section VIII concludes the paper.

II. BISTATIC GNSS RADAR SYSTEM GEOMETRY AND SIGNAL MODEL

The acquisition geometry of the proposed bistatic passive radar system is shown in Fig. 1. The transmitter is one of the assumed GNSS transmitters flying over the the receiver. R_T and R_R are the transmitter-to-target and the receiver-to-target ranges, respectively. The angle β is the solid bistatic angle defined as the angle between the transmitter, the target, and the receiver [8].

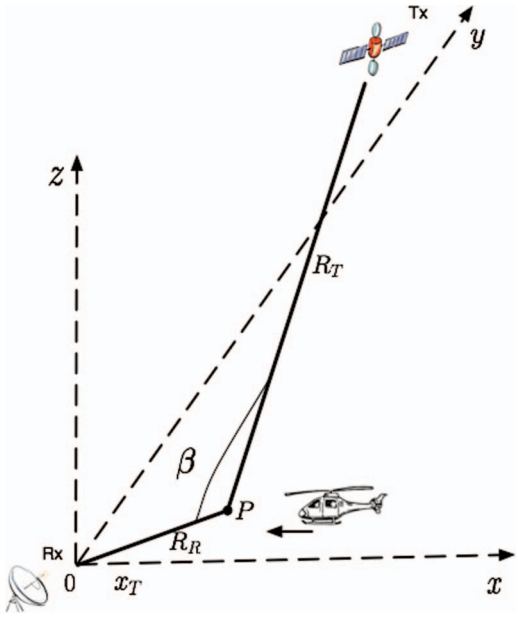

Fig. 1. Proposed bistatic passive radar geometry with GNSS illuminator.

The principal transmitted signal from the GNSS satellite is a code division multiple access code consisting of a pseudo random noise (PRN) sequence called C/A code. We concentrate on the case of the GPS constellation and consider the L_1 signal at 1.5 GHz. Each satellite can be identified based on the specific C/A sequence which exhibits a very narrow cross-correlation function allowing the system to measure the time delay between the satellite platform and the GPS receiver.

The same principle can be exploited to perform target ranging when a target scatters the signal coming from the GPS satellite to a receiver located on ground or on an aircraft. The relative delay between the reference signal, obtained as the direct signal from the satellite at the receiver on a different antenna and the scattered echo from the target can be estimated. In this paper we assume that the direct signal at the receiving antenna used to perform ranging has been removed through physical shielding, digital beamforming, or digital signal processing (DSP) techniques (8).

The received radar return after the cross-correlation with the replica of the PRN signal can be modeled as [20]

$$s_{rc}(\tau,\eta) = A_0 p_r\left(\tau - \frac{R_R(\eta)}{c}\right)\exp\left\{-j\frac{2\pi f_0 R(\eta)}{c}\right\} \tag{1}$$

where f_0 is the carrier frequency, c is the speed of light, $p_r(\tau)$ is the range envelope where the time reference is triggered to the direct signal received from the transmitter, A is the amplitude of the scattered signal, τ is the variable representing the fast time of the received signal, while η represents the slow time of the acquisition of the different echoed PRN sequences, and $R(\eta)$ is the bistatic target range. This slow time is required because the dynamics of the micro-motion is slower than the dynamics of the signal used to perform ranging. This is also the reason why the cross-correlation of the C/A sequence can be performed without affecting the micro-Doppler analysis. However the signal model requires being modified in the presence of target micro-motions where phase modulation of the signal is introduced. This aspect is analyzed in Section III.

III. MICRO-DOPPLER SIGNATURE OF HELICOPTERS ROTOR BLADES

In the application considered in this paper the receiver is a platform on ground. This kind of configuration allows us to obtain easily a near forward scattering configuration. The target is a helicopter approaching the line of sight (LOS) between the transmitter and the receiver. It means that the bistatic angle β is close to 180° where forward scattering enhancement can be obtained [8].

Fig. 2 shows a view of the geometry of the rotor blades relative to the bistatic geometry. The rotating plane of the rotor blade is parallel and orthogonal to the LOS between the transmitter and the receiver. V_{tip} is the velocity vector

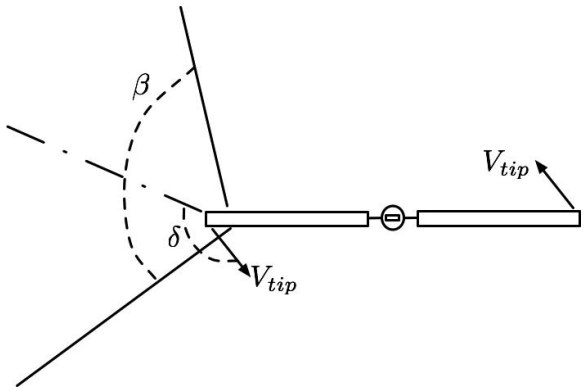

Fig. 2. Geometry of rotating blades seen from bistatic radar.

of the tip of the rotor blade and δ is the angle between V_{tip} and the bisector of the bistatic angle β. The angles β and δ are two important factors that influence the micro-Doppler signature of the target in a bistatic geometry [12].

The model of the received signal in (1) must consider also the effect of the micro-motion as follows:

$$s_{rc}(\tau,\eta) = A_1(\eta)p_r\left(\tau - \frac{R_R(\eta)}{c}\right) \times \exp\{-j(\Phi_R(\eta)+\Phi_{mD}(\eta))\} \quad (2)$$

where $\Phi_R = 2\pi f_0 R(\eta)/c$ is the phase of the target containing the constant motion and $\Phi_{mD}(\eta)$ is the phase modulation due to the micro-motions of the target and can be expressed as [12]

$$\Phi_{mD}(\eta) = -\frac{2\pi}{\lambda}\frac{L_b}{2}\cos\left(\frac{\beta}{2}\right)\cos(\delta)\cos(\Omega\eta+\theta_0) \quad (3)$$

where L_b is the length of the rotor blade, Ω is the angular rotation rate, and θ_0 is the initial rotating phase. The product $\cos(\frac{\beta}{2})\cos(\delta)$ is the factor that takes into consideration the bistatic geometry [12]. The amplitude of the received echo is also affected by the rotation of the blade and may be written as

$$A_1(\eta) = A_0 sinc\left(\frac{2\pi}{\lambda}\frac{L_b}{2}\cos\left(\frac{\beta}{2}\right)\cos(\delta)\cos(\Omega\eta+\theta_0)\right). \quad (4)$$

Assuming that a rotor has N blades they will have N different initial phases $\theta_k = \theta_0 + k2\pi/N$ with $k = 0, 1, 2, \ldots, N-1$. The total received signal from the N blades will be the sum of the modulated signal from each blade, from (2), (3), and (4) it can be written as

$$s_{\text{tot}}(\tau,\eta) = \sum_{k=0}^{N-1} A_{1_k}(\eta)p_r\left(\tau - \frac{R(\eta)}{c}\right) \times \exp\{-j(\Phi_R(\eta)+\Phi_{mD_k}(\eta))\}. \quad (5)$$

The expression is similar to the signal model in [12] but it is adapted for the specific proposed system. The micro-Doppler shift can be obtained for each blade from (3) as

$$\begin{aligned} f_{mD_k}(\eta) &= \frac{1}{4\pi}\frac{d}{d\eta}\Phi_{mD}(\eta) \\ &= \frac{L_b}{2\lambda}\Omega\cos\left(\frac{\beta}{2}\right)\cos(\delta)[-\sin(\theta_k)\sin(\Omega\eta) \\ &\quad + \cos(\theta_k)\cos(\Omega\eta)]. \end{aligned} \quad (6)$$

Equation (6) represents the expression of the expected micro-Doppler signature for a rotor blade of a helicopter of length L_b with a rotation rate Ω; it can be used then to obtain the features of the rotating blade from the micro-Doppler signature.

IV. SYSTEM REQUIREMENTS FOR MICRO-DOPPLER ANALYSIS

In a passive system with an illuminator of opportunity the carrier frequency and the sampling rate cannot be modified. These can become critical, possibly rendering the exploitation of a PBR to perform a particular micro-Doppler analysis useless. The length of the blade and the rotation rate influence the amplitude of the micro-Doppler shift. From (6) the maximum value of the micro-Doppler shift may be computed as

$$f_{mD_{\max}} = \frac{V_{tip}}{\lambda}\cos\left(\frac{\beta}{2}\right)\cos(\delta) \quad (7)$$

where $V_{tip} = 2\pi L_b\Omega$ is the velocity of the tip of a blade. From (7) the minimum sampling rate to avoid aliasing and to permit a good time-frequency analysis, is in the slow time, can be obtained. For a monostatic radar the maximum micro-Doppler shift may be expressed as [12]

$$f_{mD_{\max_{\text{mono}}}} = \frac{2V_{tip}}{\lambda}\cos(\alpha) \quad (8)$$

where α is the elevation angle of the monostatic platform. From (8) and (7) it can be seen that the bistatic micro-Doppler shift is always less than the monostatic value and therefore the minimum sampling frequency required to avoid aliasing in a bistatic radar system is smaller than that required in the monostatic case.

An additional parameter of the system that strongly influences the micro-Doppler shift is the wavelength that, if too small, will produce a very high micro-Doppler shift. For this reason very high frequencies are more useful for micro-Doppler analysis of very small micro-motions [21], while in cases such as helicopter blades a larger wavelength could help produce acceptable micro-Doppler shifts.

The wavelength used by the proposed PBR is of 19 cm, this is a very big value that can reduce the maximum micro-Doppler shift obtainable. In addition the bistatic configuration in the near forward scattering zone produces a small value of the product $\cos(\frac{\beta}{2})\cos(\delta)$ that appears in (7); this product is also helpful in reducing the maximum micro-Doppler shift. For the reasons explained above, the proposed PBR is a good candidate to perform micro-Doppler analysis of the helicopter rotor blades. For

example, a blade of length of 7.3 m rotating at 4.8 r/s observed with β of 169° and δ of 10.3° will produce a maximum micro-Doppler shift of 102 Hz that is smaller than half of the system PRF of 1 kHz, demonstrating that the proposed PBR is capable of performing micro-Doppler analysis for this kind of target.

Another aspect to be considered is related to the C/A code sensibility and interference, specifically the Doppler resolution of the C/A code in the specific configuration. In order to analyze performances of the C/A code the normalized amplitude of the AF for a sequence of the C/A code is represented in Fig. 3. The AF shows the range and Doppler resolution and the sidelobe level in both directions. In Figs. 4 and 5 a cut at 0 delay and 0 Doppler shift of the AF are shown, respectively. It can be seen how

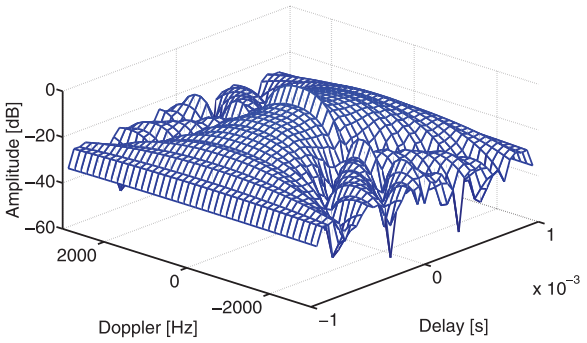

Fig. 3. 2-D AF for C/A code.

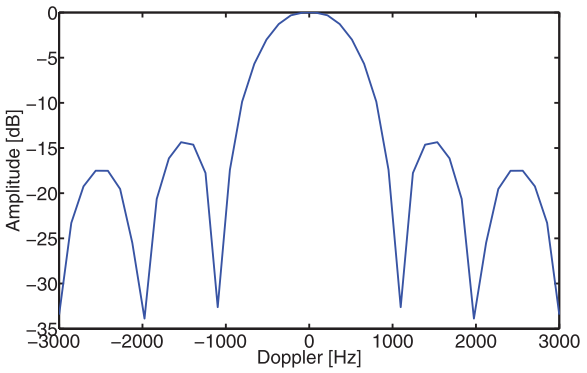

Fig. 4. AF for C/A code at 0 delay.

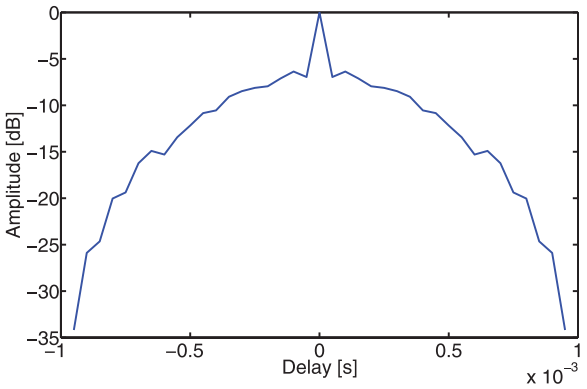

Fig. 5. AF for C/A code at 0 Doppler.

the delay resolution of the C/A code is relatively small in order to match the original application requirements of this waveform for an accurate navigation. In the Doppler domain the AF has a $sinc^2$-like shape with zero crossing at 1 kHz and a first sidelobe at 1.5 kHz at –15 dB. These aspects require further analysis for both the velocities and target detection. In this section we discuss the first of these aspects while the second one, related to the sidelobe level, is discussed in Section VI. The bistatic Doppler resolution and AF have been studied in the past [8, 12, 22], where it was demonstrated how the bistatic geometry influences the Doppler resolution.

$$\Delta f_{Bi} = \Delta f_{\text{Mono}} \cos\left(\frac{\beta}{2}\right). \tag{9}$$

From (9) [12] the effect of the bistatic angle affects the capability to detect targets with different velocities. In addition in the case of 180°, the Doppler resolution goes to 0 making it impossible to discriminate targets using Doppler signatures. However the Doppler resolution may not be sufficient in cases where different blades produce similar micro-Doppler shifts. For our purpose it is required to be able to detect the flashes in the time-frequency distribution. Whenever the Doppler resolution becomes ambiguous then the micro-Doppler shift amplitude will not be a discriminant between two helicopters, for example when two particular combinations of blade length and blade rotation velocity give a similar micro-Doppler shift, the rotating period can still be used as a discriminant and is sufficient for target classification [23].

V. FORWARD SCATTERING ENHANCEMENT

In this section we introduce the forward scattering enhancement in order to predict the bistatic RCS for the rotor blade.

The forward scattering enhancement occurs when the bistatic angle is large, i.e., near 180° [7]. When an opaque object is illuminated by an electromagnetic wave, a shadow is produced if the object dimensions of the objects are larger than the wavelength. The shadow, which occurs on the opposite side of the object from the energy source, describes a region in which the electromagnetic fields are very small. It means that the currents induced in the object by the incident wave reradiate a secondary electromagnetic wave that cancels the incident wave in the shadow region. The resulting forward-scattered radiation can be determined by integrating contributions from the induced currents. However this is very impractical, since doing so requires knowledge of the currents themselves which in turn requires knowledge that involves solving a difficult boundary value problem. For this reason the use of the equivalence theorem [24] is a solution to obtain the forward-scattered radiation. For this purpose it is required that the radiation scattered by currents induced in the object must be equal to the radiation from appropriate electrical and magnetic surface currents on an infinite plane. These surface currents are proportional to the

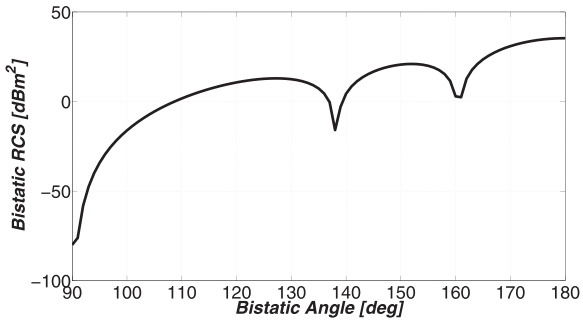

Fig. 6. Bistatic RCS for 5.5 × 0.6m rotor blade.

canceled fields in the shadow region and are zero elsewhere. By integrating the differential contributions over the plane it is possible to compute the radiation from the surface currents. Since the canceled fields on the plane are in phase, their differential contributions also add up in phase in the forward direction, resulting in a strong radiation peak. Moreover, the radiation pattern is similar to the pattern generated when the same incident fields impinge on an aperture in an opaque screen whose shape is identical to the object's shadow, or silhouette. In [25] it was shown that based on the physical optics, the forward-scatter RCS for a target with silhouette area A is

$$\sigma_{b_{\text{peak}}} = \frac{4\pi A^2}{\lambda^2} \tag{10}$$

This is principally due to the Babinet's principle, which says that the diffracted wave from a perfect absorbing target is the same as that radiated from an aperture of the same shape and area A of the target. In our case we are considering a rotor blade of length L_b and blade width W_b, then the surface area A can be replaced in (10) that becomes

$$\sigma_{b_{\text{peak}}} = \frac{4\pi (L_b W_b)^2}{\lambda^2}. \tag{11}$$

For example, Fig. 6 shows the bistatic RCS for a rectangular shaped rotor blade sized 5.5m × 0.6m.

In order to calculate the RCS of a helicopter rotor blade in literature the Phisic Optics approximation has been used [26]; in our analysis we use a simpler model of the rotor blade and the Phisic Optics to obtain the angle-dependent RCS. We used the physical optics approximation provided in the POfacets tool for Matlab® [27] simulating a flat metallic blade with the rotating plane parallel to the ground. The simulated rotating blade is illuminated on the top face from the tranmitter and the receiver looks at it from the bottom. The bistatic angle is them measured at the tip of the blade. Working in the near forward scattering zone the Babinet principle warranties that the most important part is the target silhouette and not the composition or the shape of the blade surface. In [28] the case of big bistatic angles was analyzed and a strong return from a rotor blade at 180° was demonstrated. In Fig. 6 it can be seen that for values of the bistatic angles between 165° and 180° the bistatic RCS values are higher than 20 dBsm which still represent considerable high values.

The value of the bistatic RCS of the rotor blade is a critical aspect in the proposed approach. High RCS values that are obtained in the near forward scattering zone are required to provide an acceptable maximum operative range. This aspect is analyzed in the power budget analysis developed in the next section.

VI. POWER BUDGET ANALYSIS

In [3], [4], [5] the analysis of the bistatic GPS power budget was presented, in different conditions and with different (more or less optimistic) results. In this section the analysis is contextualized in the case of the helicopter rotor blades showing that they can be detected using an appropriate system configuration within an acceptable range. The power density that reaches the receiving antenna after the scattering from the rotor blades is given by [20]

$$S_r = \left(\frac{P_t G_t}{4\pi R_T^2}\right)\left(\frac{\sigma_b}{4\pi R_R^2}\right) \tag{12}$$

where P_t is the transmitted power, G_t is the transmitter antenna gain, and, σ_b is the RCS of the rotor blade that, in our case, is increased by the forward scattering enhancement as explained in Section V. From (12) the power at the receiver after the target reflection can be expressed as

$$P_r = \left(\frac{P_t G_t}{4\pi R_T^2}\right)\left(\frac{\sigma_b}{4\pi R_R^2}\right)\left(\frac{\lambda^2 G_r}{4\pi}\right). \tag{13}$$

The first factor on the right side of (13) is the power density of the direct signal incident on the target and is termed S_{dir}. The noise at the output of the RF front-end is $N_0 = kT_{eff}BW$, where k is the Boltzmann constant, T_{eff} is the equivalent noise temperature, and BW is the bandwidth. In this power budget the losses due to processing L_{sp} and the processing gain G_{sp} are also required in order to obtain the final signal-to-noise ratio (SNR) [4]:

$$\text{SNR} = \frac{S_{dir}\sigma_b \lambda^2 G_r G_{sp}}{(4\pi)^2 L_{sp} R_R^2 k T_{eff} BW}. \tag{14}$$

For the case of a PBR another factor must be considered in the analysis: the direct signal interference (DSI). In our specific case a strong signal from the transmitting GNSS satellite will be received introducing limitations on the capability to detect a target [29]. In order to quantify the effect of DSI we introduce the signal-to-interference ratio (SIR) which is defined as the ratio between the received power from the target and the direct signal.

$$\text{SIR} = \frac{P_r}{\left(\frac{P_t G_t}{4\pi R_{TR}^2}\right)\left(\frac{\lambda^2 G_r}{4\pi}\right)} \tag{15}$$

where R_{TR} is the baseline between the transmitter and the receiver. In Fig. 7 the SIR for a 5.5 × 0.6 m rotor blade is shown. The power reflected from the target depends on the

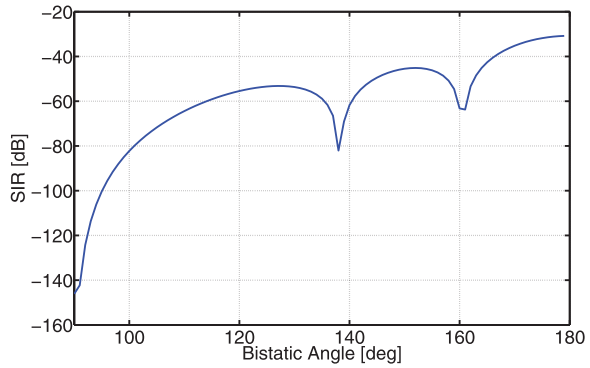

Fig. 7. SIR for 5.5 × 0.6m rotor blade.

bistatic angle since the bistatic RCS changes with it. However the SIR also depends on the bistatic configuration.

Considering a range of operative angles between 140° and 175°, then from Fig. 7 it is seen that the SIR varies between -60 and -30 dB. However this is the expected SIR in the zero Doppler. The Doppler shift from a rotor blade seen from a monostatic radar is on the order of 1500 Hz; this shift is reduced in the bistatic case. For increasing bistatic angles the Doppler shift produced by the component of the velocity vector orthogonal to the bisector of the bistatic angle results in the order of 100 Hz for helicopter rotor blades, appearing in the first sidelobe of the shrinked version of the AF in Fig. 3. For this reason 15 dB less of SIR can be considered. However a suppression strategy will still be required in order to mitigate the SIR of maximum 45 dB. Different approaches have been proposed to mitigate the SIR [29]. Existing PBR are able to work in more restrictive conditions, with stronger interference [30]. For this reason existing methods can be applied in our case. For example, in [30] a two-stage adaptive noise canceler was developed. The first stage is an adaptive M-stage lattice predictor, and the second stage is an adaptive tapped delay line. This approach provides a high level of suppression of the SIR on the order of 75 dB. The selection of the best technique for the SIR removal in our specific case goes beyond the scope of this paper and will be addressed in the future. From the discussion above it is now possible to compute the maximum achievable range assuming a minimum signal-to-interference-and-noise ratio (SINR) value, defined as

$$\text{SINR} = \frac{P_r}{\frac{P_t G_t}{4\pi R_{TR}^2}\frac{\lambda^2 G_r}{4\pi} + kT_{eff}BW}. \tag{16}$$

The maximum range that can be obtained is

$$R_{R_{\max}} = \sqrt{\frac{S_{dir}\sigma_b \lambda^2 G_r G_{sp}}{(4\pi)^2 L_{sp} \text{SINR}_{min} kT_{eff} BW}}. \tag{17}$$

The values to be used in (17) to obtain the maximum range for the application under consideration are shown in Table I. These values differ from the one used in [4]. In that paper a processing gain of 63 dB was assumed. This gain is not acceptable for the micro-Doppler analysis where the integration time is limited by the time coherence of the specific target. For this reason the 40 dB gain coming from the C/A code cross-correlation is considered and 13.2 dB is added assuming a 21 ms integration time. Due to this decrease in the processing gain a 25 dB receiver antenna gain is considered. The RCS of the rotor blade with blade length L_b and blade width W_b is considered to be ten times less than the peak RCS obtainable in the forward scattering configuration from (11). From the parameters in Table I the maximum range is on the order of 2.4 km. This is a reasonable distance to have an effective near forward scattering configuration for this kind of PBR.

TABLE I
Simulated Parameters in the Power Budget Analysis

Parameter	Value	Units
S_{dir}	39.81×10^{-15}	W/m^2
L_b	5.5	m
W_b	0.6	m
σ_b	379	m^2
SINR_{min}	8	dB
Bandwidth	2.046×10^6	Hz
T_{eff}	344	K
λ	0.19	m
G_{sp}	53.2	dB
L_{sp}	3.25	dB
G_r	25	dB
k	1.30×10^{-23}	
$R_{\max}$	2420	m

VII. SIMULATIONS AND RESULTS

In this section the results obtained simulating the rotor blades of different helicopters using the proposed PBR are presented. Results that compute the maximum range for different helicopters based on the rotor blades parameters given in Table II and the power budget parameters (excluding the RCS) in Table I are now presented.

In Fig. 8 the maximum ranges obtained for the four helicopters are shown. It can be seen that the maximum range increases as the bistatic gets closer to 180°. It can be seen from Fig. 8 that for smaller rotor blades, like in the case of the Defender, the maximum range is smaller, while for bigger blades, like those of the Black Hawk, the maximum range becomes larger as it is able to exploit the forward scattering enhancement in a superior fashion.

In Fig. 9 the resulting SIRs for the four helicopters rotor blades at a range distance of 4 km from the receiver is shown. It can be seen how for each of the helicopters we obtain a wide range of angles where the power reflected from the blades reduces the interference due to the forward scattering enhancement.

Numerical values for the simulated geometry shown in Fig. 1 are given in Table III where the helicopter is located in P. The geometry simulates the case where the helicopter is approaching the baseline leading to the condition that

TABLE II
Simulated Helicopters Rotor Blades Features and Target Parameters for the Configuration in Table III

Model	AW-109 Agusta	AH-64 Apache	UH-60 Black Hawk	MD 500E Defender
# of blades	4	4	4	5
Blade length [m]	5.5	7.3	8.18	4
Blade width [m]	0.6	0.6	0.6	0.6
Rotor vel. [r/s]	7	4.8	4.3	8.2
Tip velocity [m/s]	241.90	220.16	221.00	206.08
Maximum m-D shift [Hz]	112.24	102.13	102.52	95.60
RCS [dBsm]	25.76	28.2	29.2	22.9

can produce forward scattering enhancement. This condition seems to be very particular and restrictive, however with a high degree of probability, there are generally three or four satellites illuminating the same area, thus increasing the probability to have such a configuration. In Table II the characteristics of the four simulated helicopters are provided. It can be seen that they have different blade length and rotation velocity and three of them have an even number of blades while one has an odd number of blades. The table provides also the maximum micro-Doppler shift expected in the case of the simulated geometry using the parameters given in Table III. It can be seen that despite the different features of the helicopters, the interval containing the maximum micro-Doppler is very small. However we show that it remains sufficient to discriminate between the different helicopters.

Figs. 10(a), 11(a), 12(a), and 13(a) show the amplitude of the radar return from the rotor blades of the four helicopters. These clearly show that the radar return is composed of flashes that repeat with an interval equal to

TABLE III
Simulated Geometry

X_T	0	m
Y_T	0	m
Z_T	20200×10^3	m
X_R	0	m
Y_R	0	m
Z_R	0	m
X_P	400	m
Y_P	0	m
Z_P	2200	m
β	169.69	deg
δ	10.30	deg

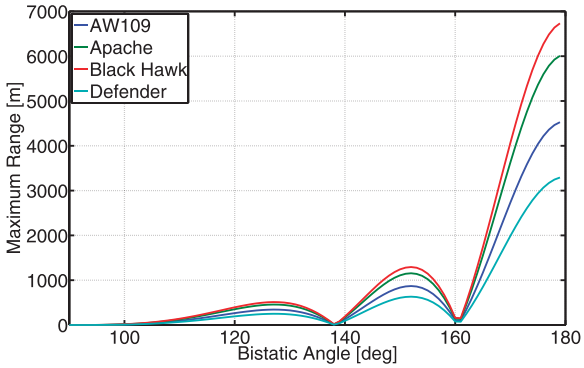

Fig. 8. Maximum range for helicopters in Table II with parameters in Table I.

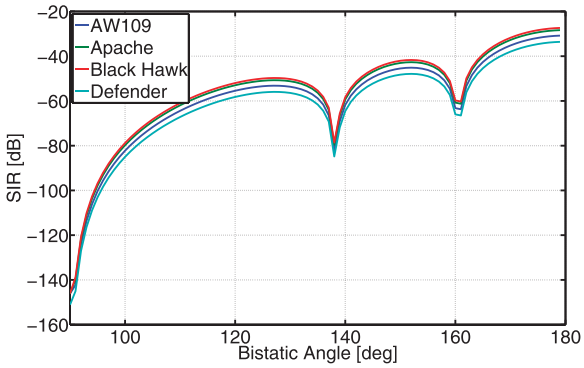

Fig. 9. SIR for helicopters in Table II with parameters in Table I.

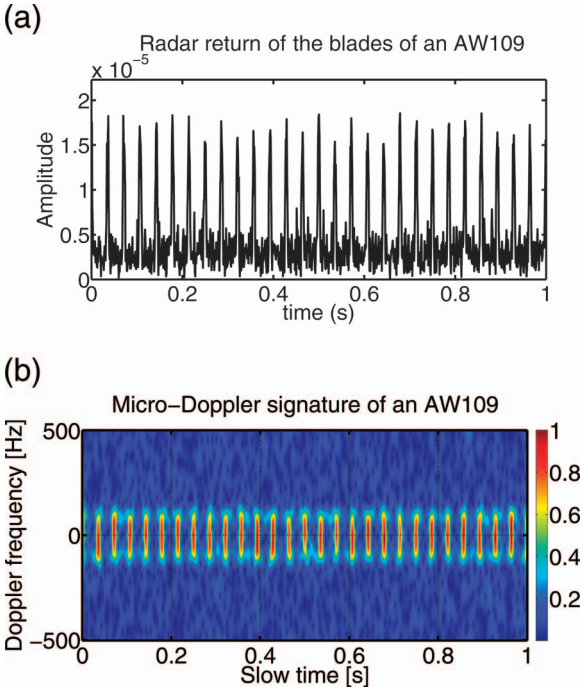

Fig. 10. (a) Radar return and (b) micro-Doppler signature for an AW109.

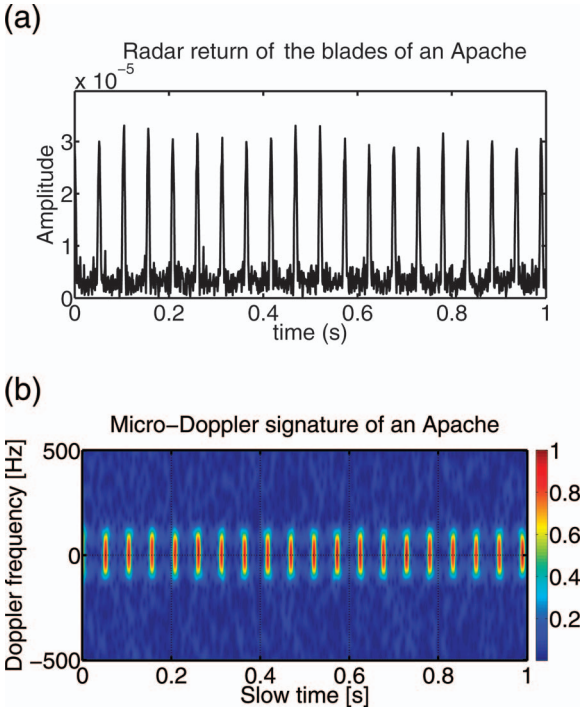

Fig. 11. (a) Radar return and (b) micro-Doppler signature for an Apache.

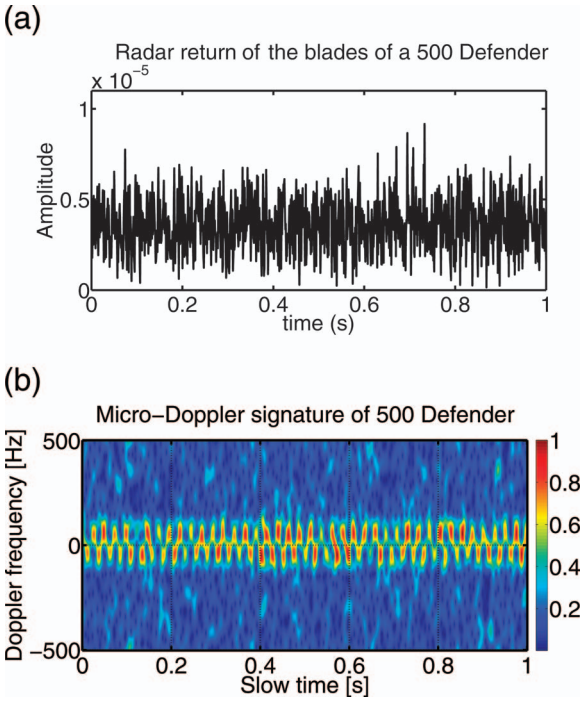

Fig. 13. (a) Radar return and (b) micro-Doppler signature for a Defender.

the rotation frequency of the rotor blades divided by the number of blades. However this is the only information about the rotor feature that can be obtained from this plot; for a more accurate, complete and useful analysis a time-frequency analysis is required. From Fig. 13(a) it can be seen that the signal is more affected by noise principally due to the smaller RCS of the rotor blades that are actually smaller as can be seen from the data reported in Table II. For this reason the analysis of the radar return amplitude is very difficult and almost useless for our purpose.

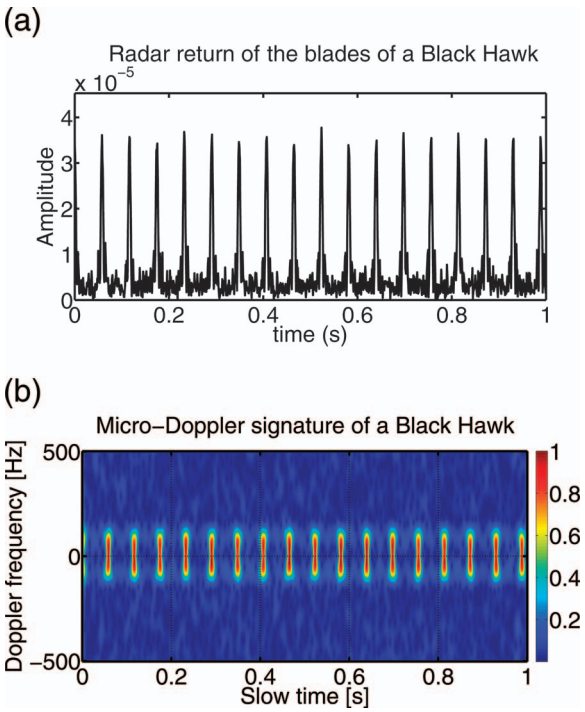

Fig. 12. (a) Radar return and (b) micro-Doppler signature for a Black Hawk.

In Figs. 10(b), 11(b), 12(b), and 13(b) the micro-Doppler signature of the simulated received signal from each of the helicopters rotors is shown. The time-frequency analysis is performed using the short time Fourier transform using a Hamming window of the duration of 21 ms.

For the helicopters with an even number of blades, from Figs. 10(b), 11(b), and 12(b) it can be seen that flashes in both the positive and negative Doppler appears. This is due to the symmetry of the rotor meaning that while a blade is approaching the receiver the one on the same axis of the rotor is receding from the receiver, then two blades at the same time will produce the same micro-Doppler shift at the same time but with different sign. In Fig. 13(b) the flashes are not aligned, this is because the number of blades is odd. It means that there will not be two blades with the velocity vector V_{tip} parallel to the bisector of the bistatic angle β at the same time. For the case shown in Fig. 10 the period of the rotation can be obtained from the flashes and is measured to be of 0.1432 s corresponding to 6.9832 rev/s, close to the original 7 rev/s. The maximum amplitude of the micro-Doppler shift measured at the -3 dB point is of 112.5 Hz. From this information the following formula can be obtained from (7) and can be used to estimate the blade length:

$$\hat{L}_b = \frac{\hat{f}_{mD_{max}}\lambda}{\cos\left(\frac{\beta}{2}\right)\cos(\delta)2\pi\hat{\Omega}} \tag{18}$$

where $\hat{f}_{mD_{\max}}$ and $\hat{\Omega}$ are the estimated maximum Doppler shift and rotation rate, respectively. From (18) for the case of the Agusta AW109 the estimated blade length results in 5.5268 m, a value very close to the simulated value in Table II. For the case of the Apache in Fig. 11 the measured rotation rate is of 4.78 rev/s, while the maximum micro-Doppler results in 97.39 Hz leading to an estimated blade length of 6.98 m; the error is principally due to the choice of frequency bins in the time-frequency analysis. The measured rotation rate for the Black Hawk in Fig. 12 is of 4.29 rev/s, while the maximum micro-Doppler results in 102.4 Hz leading to an estimated blade length of 8.1887 m; again the micro-Doppler signature is good to extract the features of the rotor blades. The last case is the case in Fig. 13 with 5 blades. In this case the measured rotating rate is 8.1566 rev/s and the maximum micro-Doppler frequency results in 97.39 Hz; these values lead to obtaining a blade length of 4.0962 m that is a good estimation of the original length.

VIII. CONCLUSIONS

This paper investigated the possibility of exploiting the GNSS signal in a PBR system when a target is in the near forward scattering zone for micro-Doppler analysis. The feasibility study has provided the power budget analysis showing that by exploiting the forward scattering enhancement it is possible to obtain enough forward-scattered power from the rotor blades of a helicopter. The feasibility study investigated the micro-Doppler characteristics of the echoes received from the rotating blades, showing that this particular system operating in the near forward scattering zone allows useful analysis of the micro-Doppler signatures.

The proposed PBR system has been simulated and the presence of different helicopters flying in the near forward scattering zone has been simulated. The micro-Doppler signature relative to their rotor blades in this kind of system has been analyzed and the possibility to extract the rotor blades features from it has been shown with a good confidence in the possibility to recognize the specific helicopter. The proposed PBR is therefore a good candidate to be an alternative application of the GNSS signal and is useful for the analysis of the micro-Doppler signatures of helicopters and can find applications in areas such as borders or coastal surveillance.

REFERENCES

[1] Gleason, S. and Gebre-Egziabher D.
GNSS Applications and Methods. Norwood, MA: Artech House, 2009.

[2] Cherniakov, M.
Bistatic Radar: Emerging Technology. Hoboken, NJ: Wiley, 2008.

[3] He, X., Zeng, T., and Cherniakov, M.
Signal detectability in SS-BSAR with GNSS non-cooperative transmitter.
IEE Proceedings - Radar, Sonar and Navigation, **152**, 3 (June 2005), 124–132.

[4] Dempster, A. G., Glennon, E. P., and Rizos, C.
Feasibility of air target detection using GPS as a bistatic radar.
Journal of Global Positioning System, **5**, 1-2 (2006).

[5] Mojarrabi, B. et al.
Power budget study for passive target detection and imaging using secondary applications of GPS signals in bistatic radar systems.
In *IEEE International Geoscience and Remote Sensing Symposium*, 2002 (IGARSS '02), vol. 1, pp. 449–451.

[6] Antoniou, M., Saini, R., and Cherniakov, M.
Results of a space-surface bistatic SAR image formation algorithm.
IEEE Transactions on Geoscience and Remote Sensing, **45**, 11 (2007), 3359–3371.

[7] Glaser, J.
Forward scatter radar for future systems.
WSTIAC Quarterly, **10**, 3 (Mar. 2011).

[8] Willis, N.J.
Bistatic Radar. Norwood, MA: Artech House, 1995.

[9] Koch, V. and Westphal, R.
A new approach to a multistatic passive radar sensor for air defense.
In *Record of the IEEE 1995 International Radar Conference*, May 1995, pp. 22–28.

[10] Suberviola, I., Mayordomo, I., and Mendizabal, J.
Experimental results of air target detection with a GPS forward-scattering radar.
IEEE Geoscience and Remote Sensing Letters, **9**, 1 (Jan. 2012), 47–51.

[11] Chen, V.C. et al.
Micro-Doppler effect in radar: Phenomenon, model, and simulation study.
IEEE Transactions on Aerospace and Electronic Systems, **42**, 1 (2006), 2–21.

[12] Chen, V.
Micro-Doppler Effect in Radar (1st ed.). Norwood, MA: Artech House, 2011.

[13] Clemente, C. and Soraghan, J. J.
Vibrating target micro-Doppler signature in bistatic SAR with a fixed receiver.
IEEE Transactions on Geoscience and Remote Sensing, **50**, 8 (Aug. 2012), 3219–3227.

[14] Smith, G. E. et al.
Multistatic micro-Doppler radar signatures of personnel targets.
IET Signal Processing, **4**, 3 (June 2010), 224–233.

[15] Bilik, I., Tabrikian, J., and Cohen, A.
GMM-based target classification for ground surveillance Doppler radar.
IEEE Transactions on Aerospace and Electronic Systems, **42**, 1 (Jan. 2006), 267–278.

[16] Bilik, I. and Khomchuk, P.
Minimum divergence approaches for robust classification of ground moving targets.
IEEE Transactions on Aerospace and Electronic Systems, **48**, 1 (Jan. 2012), 581–603.

[17] Smith, G. E., Woodbridge, K., and Baker, C. J.
Radar micro-Doppler signature classification using dynamic time warping.
IEEE Transactions on Aerospace and Electronic Systems, **46**, 3 (July 2010), 1078–1096.

[18] Barber, B.C.
Imaging the rotor blades of hovering helicopters with SAR. In *IEEE Radar Conference (RADAR '08)*, May 2008, pp. 1–6.

[19] Cilliers, A. and Nei, W. A. J.
Helicopter parameter extraction using joint time-frequency and tomographic techniques.
In *Proceedings of the International Conference on Radar*, Sept. 2008, pp. 598–603.

[20] Skolnik, M. I.
Introduction to Radar Systems. New York: McGraw-Hill, 1981.

[21] Ruegg, M., Meier, E., and Nuesch, D.
Vibration and rotation in millimeter-wave SAR.
IEEE Transactions on Geoscience and Remote Sensing, **45**, 2 (2007), 293–304.

[22] Tsao, T. et al.
Ambiguity function for a bistatic radar.
In *Proceedings of the IEEE-SP International Symposium Time-Frequency and Time-Scale Analysis*, Oct. 1992, pp. 497–500.

[23] Molchanov, P. et al.
Classification of ground moving radar targets by using joint time-frequency analysis.
In *IEEE Radar Conference (RADAR)*, May 2012, pp. 0366–0371.

[24] Felsen, L. P., Mongiardo, M., and Russer, P.
Electromagnetic Field Computation by Network Methods.
New York: Springer, 2009.

[25] Siegel, K.
Bistatic radars and forward scattering.
In *Proceedings of the National Conference on Aeronautical Electronics*, May 1958, pp. 286–290.

[26] Pouliguen, P. et al.
Calculation and analysis of electromagnetic scattering by helicopter rotating blades.
IEEE Transactions on Antennas and Propagation, **50**, 10 (Oct. 2002), 1396–1408.

[27] Radar cross section calculations using the physical optics approximation, pofacets.
Available: http://faculty.nps.edu/jenn/

[28] Pouliguen, P., Damiens, J. F., and Moulinet, R.
Radar signatures of helicopter rotors in great bistatism.
In *IEEE Antennas and Propagation Society International Symposium*, June 2003, vol. 3, pp. 536–539.

[29] Griffiths, H. and Baker, C.
The signal and interference environment in passive bistatic radar.
In *Information, Decision and Control Conference (IDC '07)*, Feb. 2007, pp. 1–10.

[30] Howland, P. E., Griffiths, H. D., and Baker, C. J.
Passive bistatic radar systems. In M. Cherniakov (Ed.), *Bistatic Radar: Emerging Technology*. Hoboken, NJ: Wiley, 2008, ch. 7.

Carmine Clemente (S'08-M'13) received the Laurea cum laude (BSc) and Laurea Specialistica cum laude (MSc) degrees in telecommunications engineering from Universita degli Studi del Sannio, Benevento, Italy, in 2006 and 2009, respectively. In 2012, he received the Ph.D. degree in the Dept. of Electronic and Electrical Engineering, University of Strathclyde, Glasgow, UK., where currently he is a research associate working on advanced radar signal processing algorithms, MIMO radar systems, and micro-Doppler analysis. His research interests include synthetic aperture radar (SAR) focusing and bistatic SAR focusing algorithms development, micro-Doppler signature analysis and extraction from multistatic radar platforms, micro-Doppler classification, statistical signal processing, and high-performance computing.

John J. Soraghan (S'83-M'84-SM'96) received the B.Eng. (Hons.) and M.Eng.Sc. degrees in electronic engineering from University College Dublin, Dublin, Ireland, in 1978 and 1983, respectively, and the Ph.D. degree in electronic engineering from the University of Southampton, U.K., in 1989.

After graduating he worked with the Electricity Supply Board in Ireland and with Westinghouse Electric Corporation in the United States. In 1986 he joined the Dept. of Electronic and Electrical Engineering, University of Strathclyde, Glasgow, U.K., as a lecturer and became a senior lecturer in 1990, a reader in 2000, and a professor in signal processing in Sept. 2003, within the Institute for Communications and Signal Processing (ICSP). In December 2005 he became the head of the ICSP. He currently holds the Texas Instruments Chair in Signal Processing with the University of Strathclyde. He was a manager of the Scottish Transputer Centre from 1988 to 1991, and a manager of the DTI Parallel Signal Processing Centre from 1991 to 1995. His main research interests are signal processing theories, algorithms and architectures with applications to remote sensing, telecommunications, biomedicine, and condition monitoring.

Prof. Soraghan is a member of the Institution of Engineering and Technology.